Influence of Sigma Phase on Hydrogen Induced Cracking of Duplex Stainless Steel

KURODA Toshio* , IKEUCHI Kenji** , NAKADE Katsuyuki***

Abstract

New software for the 3-dimensional reconstruction of the image of the fracture surface from a stereo-pair of SEM photographs was developed using a personal computer. This software was applied to clarify the effect of sigma phase on hydrogen induced cracking of SUS329J1 duplex stainless base metal.

The hydrogen induced cracking was recognized in the as-received SUS329J1 base metal and showed quasi-cleavage fracture. The cross-sectional microstructure observation directly revealed that hydrogen induced cracking occurred in ferrite, while austenite showed ductile fracture. The sigma phase enhanced hydrogen embrittlement and many secondary cracks due to sigma phase were observed.

Sigma phase was observed for the sample heated at 1023K for 72ks. The existence area of sigma phase was always the bottom area and lower than other areas on the 3-dimensional fracture surface and indicated that sigma phase strongly promoted hydrogen induced cracking.

According to the cross-sectional microstructure observation, it was found that sigma phase itself and sigma/ferrite phase boundaries were preferential initiation sites of hydrogen induced cracking, while quasi-cleavage fracture assisted hydrogen induced cracking in the SUS329J1 base metal.

KEY WORDS : (Duplex stainless steel) (Sigma phase) (Ferrite) (Austenite) (Hydrogen Induced cracking) (3-dimensional reconstruction image)

1. Introduction

Duplex stainless steels are suitable for many marine and petrochemical applications, particularly where chlorides are present [1]. It has been reported that duplex stainless steel containing ferrite is subject to hydrogen embrittlement [2)-3)] and fisheyes has been observed and welding cracks associated with hydrogen levels greater than 7ppm in Ferralium 259 duplex stainless weld metal [4].

On the other hand, sigma phase can be observed in the temperature range 573K-1323K [1] and sigma phase is by far the most important because of its large volume fraction, and its profound influence on toughness.

Sigma phase having a tetragonal structure is basically a Fe-Cr-Mo intermetallic compound and precipitates very quickly by reheating since higher Cr and Mo are added for improving resistance to pitting corrosion. However, the effect of sigma phase on hydrogen induced cracking was not examined.

Fractography techniques can provide direct evidence of the fracture process in the analysis of suffering components in-service cracking. Many experiments have been done using the scanning electron microscope (SEM), mainly because observable magnifications (from 40 times to 10 thousand times on average) are wide and very rough surfaces can be analyzed because of the high depth of focus [5)-7)], However, the main analysis involved the determination of the features of the fracture pattern; for instance, dimple or brittle or understanding of macro fracture propagation direction etc. For increasing the understanding of the fracture process, a 3-dimensional image was observed in a stereoscopic viewer to discover information associated with fracture surface elevation. However, such images are dependent on the viewer and cannot provide

† Received on November 10, 2002
* Associate Professor
** Professor
*** Graduate Student

Transactions of JWRI is published by Joining and Welding Research Institute of Osaka University, Ibaraki, Osaka 567-0047, Japan

quantitative topography.

With such a background, accurate 3-dimensional topography was built up and then used to examine the effect of sigma phase on hydrogen induced cracking.

In addition, 3-dimensional fracture analysis was proposed for advanced fracture analysis [1)-2)].

2. Experimental Procedure

The base metals used in this investigation are shown in **Table 1**.

The specimens were reheated at 1023K for various times in order to precipitate sigma phase. Microstructural observation was carried out after electrolytic etching in 10kmol/m^3 KOH solution. The etching technique colored sigma phase brown, colored ferrite blue and colored austenite white. In the case of monochrome photographs, the etching technique colored sigma phase black, colored ferrite gray and colored austenite white.

The notch tensile test was conducted at a slow strain rate of 0.1mm/min (0.016mm/s) to investigate the effect of sigma phase. Hydrogen was added to the tensile specimen by the cathodic charging technique in a solution of 5% H_2SO_4 with a small amount of $NaAsO_2$ as a catalytic poison. Current density was 2000A/m^2 and charging time of 7.2ks was employed.

The reconstruction of a 3-dimensional image consists of searching a corresponding point on the two stereographs so that the elevation can be computed by measuring relative displacement. We adopted an area-based matching or template matching algorithm to find corresponding regions.

Fig.1 shows the template matching method. This method consists of the extraction of small square windows (called the window areas) from stereo pair images to find corresponding regions. The position search algorithm used was both SSDA method and MCC method. SSDA method is known as a fast algorithm, which terminate calculation just after the sum of differences in gray level become more than a threshold value and then advance to the next calculation. One small window area is extracted from the standard image and then R(m,n) is calculated by superimposing this extracted window area into the search area of oblique image in MCC method.

The coefficient of correlation is calculated on candidate points of the search area in the MCC calculation. The cross-correlation coefficient of the two windows is calculated by the following equation.

$$R(m,n)=\frac{\sum_{j=0}^{J-1}\sum_{i=0}^{I-1}(W(i,j)-\overline{W})(S(m+i,n+j)-\overline{S}(m,n))}{\sqrt{\sum_{j=0}^{J-1}\sum_{i=0}^{I-1}(W(i,j)-\overline{W})^2}\sqrt{\sum_{j=0}^{J-1}\sum_{i=0}^{I-1}(S(m+i,n+j)-\overline{S}(m,n))^2}}$$

$$=\frac{\sum_{n=0}^{N-1}\sum_{m=0}^{M-1}(W(i,j)S(i+m,j+n))-IJ\overline{W}\,\overline{S}(i,j)}{\sqrt{\sum_{j=0}^{J-1}\sum_{i=0}^{I-1}(W(i,j)^2-IJ\overline{W}^2)}\sqrt{\sum_{j=0}^{J-1}\sum_{i=0}^{I-1}(S(m+i,n+j)^2-IJ\overline{S}(m,n)^2)}}$$

where W (i,j) and S (m+i,n+j) are the gray levels of each pixel in the windows placed on the standard image and the oblique image respectively, and the average gray levels of each window which are represented by

$$\overline{W}=\frac{1}{IJ}\sum_{j=0}^{J-1}\sum_{i=0}^{I-1}W(i,j),\ \overline{S}(m,n)=\frac{1}{IJ}\sum_{j=0}^{J-1}\sum_{i=0}^{I-1}S(m+i,n+j).$$

The center pixels of the window area on standard image and oblique image were defined as a corresponding regions when the coefficient of correlation became a maximum value. The elevation of the fracture surface can then be calculated by measuring the relative displacement of corresponding points of the two images, by substituting in following equation as shown in **Fig. 2**.

The system is running under microsoft Visual Basic or Microsoft Visual C++ of windows 2000 in a 1GHz intel Pentium III personal computer. The calculated elevation data was output as a csv file and then 3-dimensional topography was displayed on a personal computer.

Table 1 Chemical composition of SUS329J1 duplex stainless steel (mass%).

Material	C	Si	Mn	P	S	Ni	Cr	Mo	N
SUS329J1	0.014	0.52	0.31	0.030	0.006	4.64	24.92	1.81	0.14

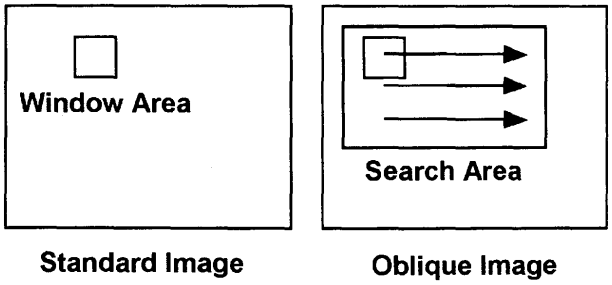

Fig.1 Schematic illustration of searching method.

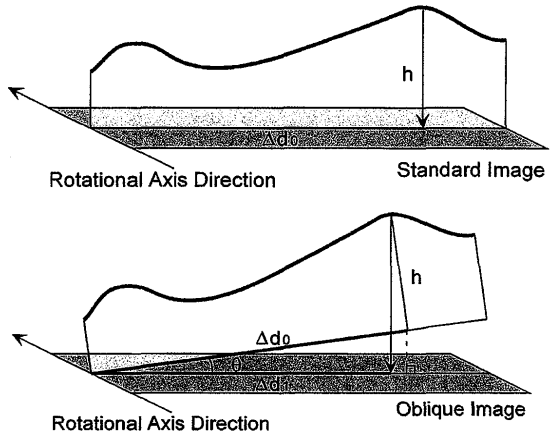

Fig.2 Schematic illustration of topography along the cross section.

3. Results and Discussion

Fig.3 shows optical micrographs for SUS329J1 base metal. The sigma phase began to precipitate at ferrite(α)/primary austenite(γ) phase boundaries and grew into ferrite. At 1023K, sigma phase began to precipitate at 3.6ks. After reheating at 1023K for 72ks, SUS329J1 base metal was primary austenite(γ) and fine secondary austenite(γ*) and sigma phase, the ferrite matrix decomposed into sigma phase and secondary austenite(γ*) as shown in Fig.3(b). After reheating at 1023K for 72ks, the area fraction of sigma phase was 25.4%. The fine secondary austenite (γ*) formation could also be observed in the ferrite matrix. The secondary austenite(γ*) formation was induced because precipitation of sigma phase depletes the adjoining ferrite matrix of chromium and molybdenum and enriches it with nickel and nitrogen. The secondary austenite enriches adjoining ferrite matrix with chromium and molybdenum, which promotes the precipitation of sigma phase.

Fig.4 shows the relation between notch tensile strength and reheating time at 1023K for SUS329J1 base metal. In the case of the hydrogen free specimen, the notch tensile strength was lowered to nearly 950MPa by sigma phase precipitation. Even if hydrogen charging was not carried out, sigma phase was found to enhance embrittlement.

After hydrogen charging, the notch tensile strength was drastically lowered with increasing sigma phase. A small reduction from 1230MPa to 1170MPa was recognized in the case of as-received base metal, It can been seen that a reduction of more than 200MPa was observed as compared to uncharged material after 72ks hydrogen charging because of the sigma phase and hydrogen addition. The difference of strengh between hydrogen free and hydrogen containing specimen was gradually increased with increase sigma phase.

It was cleared from Fig.4 that the sigma phase enhanced hydrogen embrittlement. In order to investigate in detail the hydrogen embrittlement

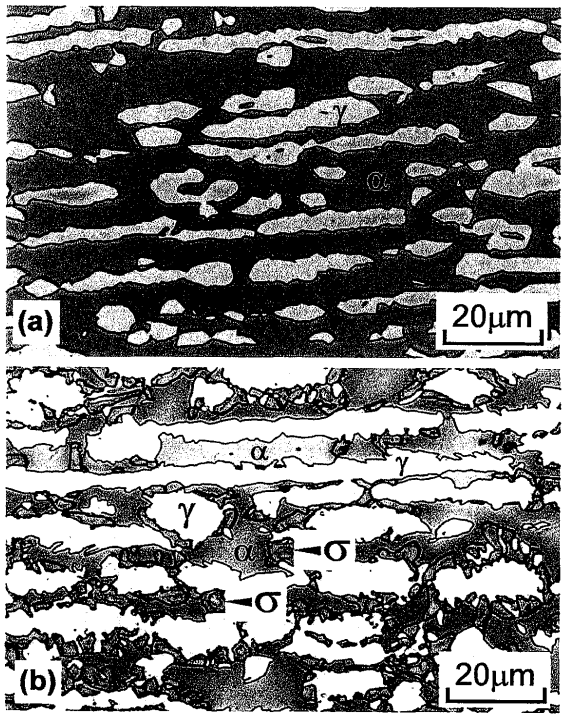

Fig.3 Optical micrographs for SUS329J1 base metal
(a): As received
(b): Heated at 1023K for 72ks.

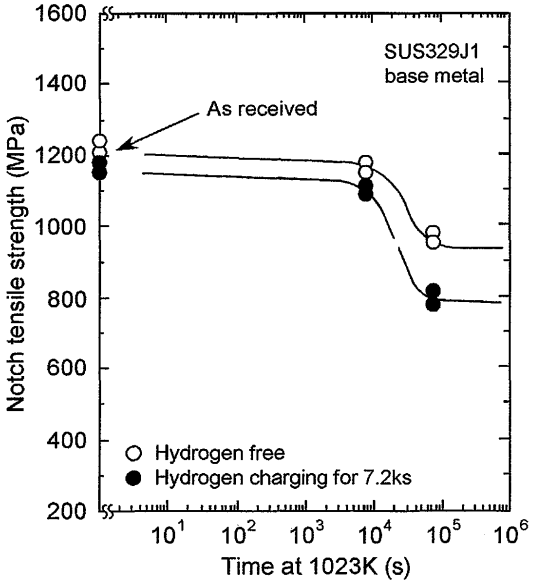

Fig.4 Variation of notch tensile strength with reheating time for SUS329J1 base metal.

Fig.5 shows a pair of stereographs of a hydrogen embrittlement fracture surface for SUS329J1 duplex stainless steel base metal. The macro-crack propagated from a notched portion to inside the specimen, hydrogen embrittlement occurred in the 200μm region from notched portion because hydrogen diffused from the notch region into internal areas of the specimen. The fracture surface consists of a brittle region and a ductile region. Hydrogen quasi-cleavage fracture surface in the ferrite phase was dominant, while white continuous lines formed by ductile fracture associated with austenite were observed in between individual hydrogen quasi-cleavage fracture surfaces.

Fig.6 shows a 3-dimensional reconstructed image (a) of the fracture surface and 2-dimensional cross sectional micrograph (b) along the cross section A-A' in Fig.5 for hydrogen-charged SUS329J1 base metal (as-received).

The conditions of calculation were as follows, [Resolution : 600dpi, tilting angle : 4° , the interval of calculating point : 10 pixel , Window area : 120 x 120 pixel , Search area : 280 x 170 pixel]

Several flat steps having the elevation differences could be observed and these differences are dependent on microstructure.

Consequently, it was clear from the 3-dimensional image that several hydrogen induced cracks propagated simultaneously in parallel directions, i:e the hydrogen quasi-cleavage fracture was not only one crack growth but also several flat hydrogen quasi-cleavage cracks having several elevations. The individual cracks occured vertical to the tensile stress direction. The mark 2-4 in Fig.5-(b) is equal to mark 2-4 in Fig.5-(a).

In order to investigate the effect of microstructure on hydrogen induced cracking, the direct cross sectional microstructure of the inspected area was examined as shown in Fig.6 (b). A little secondary crack was observed in the mark 6 in Fig.6 (b) and it could be observed that the secondary crack propagated in the ferrite and originated at ferrite/austenite phase boundaries also propagating toward the ferrite phase.

Different elevation depended on two-phase microstructure and the step corresponded to the elevation difference between the flat hydrogen quasi-cleavage plane of ferrite (blue) and ductile fractured austenite (white) edge.

It was apparent that hydrogen induced cracking propagated preferentially in the continuous ferrite at first and then ductile fracture of austenite occurred.

In the all cross sectional microstructures, the secondary crack propagated in the ferrite phase (Mark (A)). This phenomenon means that the ferrite phase in the duplex base metal is easily subjected to hydrogen embrittlement as well as ferritic stainless steel.

Fig.6(b) revealed obviously that individual steps

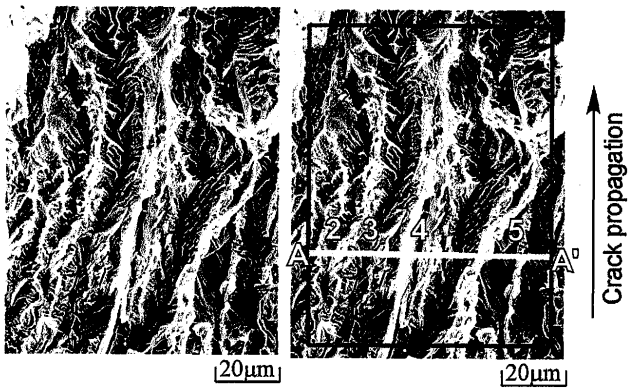

Fig.5 A pair of stereographs of the fracture surface for hydrogen-charged SUS329J1 steel.

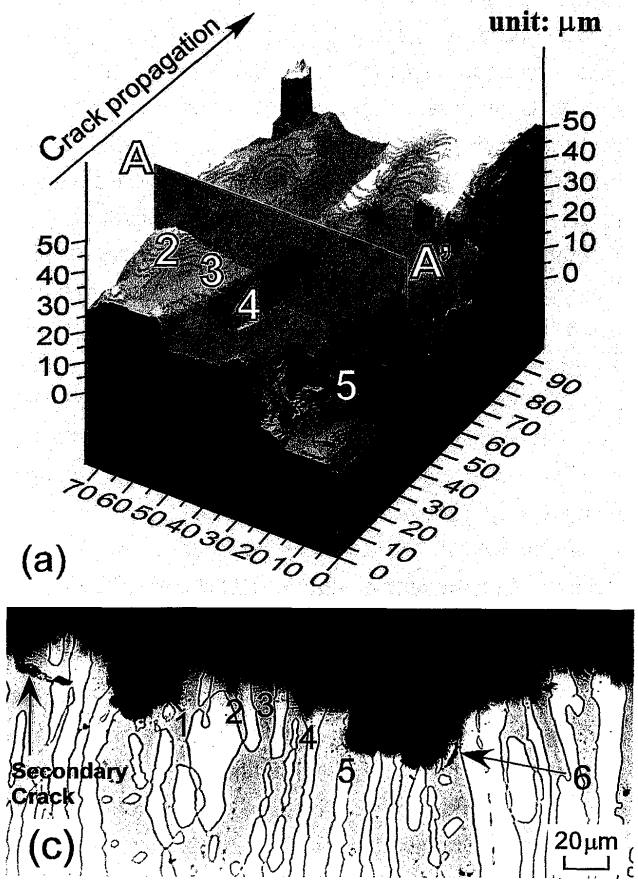

Fig.6 3-dimensional image of fracture surface (a), 2-dimensional cross sectional micrograph (b) for hydrogen- charged SUS329J1 steel.

corresponded to the typical fracture pattern of ferrite.

Furthermore, the continuous white tear ridge lines were formed by austenite and it could be confirmed that the elevation differences corresponded to distances between individual hydrogen induced quasi-clevage planes and fractured austenite edge. The elevation difference of 15μm~20μm was detected almost perpendicularly to the crack propagation direction.

The crack propagated from the front of this paper to the reverse side in the Fig.6 (b) and the hydrogen induced cracking mainly propagated in the ferrite, while austenite showed small amounts of tear ridge as a result of ductile fracture.

Fig.7 shows a pair of stereographs of hydrogen charged fracture surfaces for SUS329J1 base metal reheated at 1023K for 72ks. Before hydrogen-charging, many secondary cracks (mark 2, 4) were observed and these types of crack are associated with interaction between sigma phase and hydrogen. According to the microstructure observation, after reheating at 1023K for 72ks, the amount of sigma phase was 25.4% since ferrite decomposed into secondary austenite and sigma phase. The precipitation of sigma phases occurred at ferrite(α)/austenite(γ) phase boundaries and then grew into ferrite. By comparing the relation between sigma phase distribution and the position of the secondary crack, the main hydrogen embrittlement was assumed to occurr at the site of sigma phase.

Fig.8 shows a 3-dimensional reconstructed image (a) and the 2-dimensional image along the cross sectional L-L'(b).

The 3-dimensional image showed steep peaks and trough although it looked like a flat fracture surface. It was clear that the areas of secondary cracks are always lower than other areas, and the fracture of these areas seemed to occurr preferentially.

Fig.8(b) shows 2-dimensional peaks and trough at a constant distance and this distance is attributed to microstructure. As compared to as-received specimens, many elevation changes caused by continuous secondary cracks were observed. These secondary crack sites are mainly attributed to sigma phase. The interval between individual marks 1,2,3,4,5 was approximately 10 μm.

It is revealed that several valley surfaces (mark 2, 4) were the sites of secondary cracks from hydrogen embrittlement and also corresponded to the sites of sigma phase precipitation.

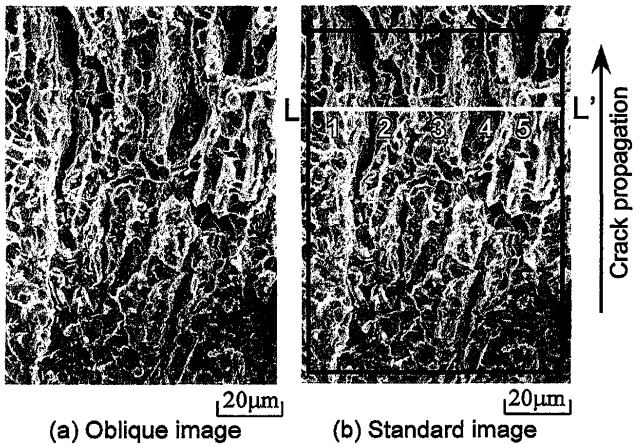

Fig.7 A pair of stereographs of fracture surface of hydrogen-charged fracture surface for SUS329J1 steel reheated at 1023K for 72ks.

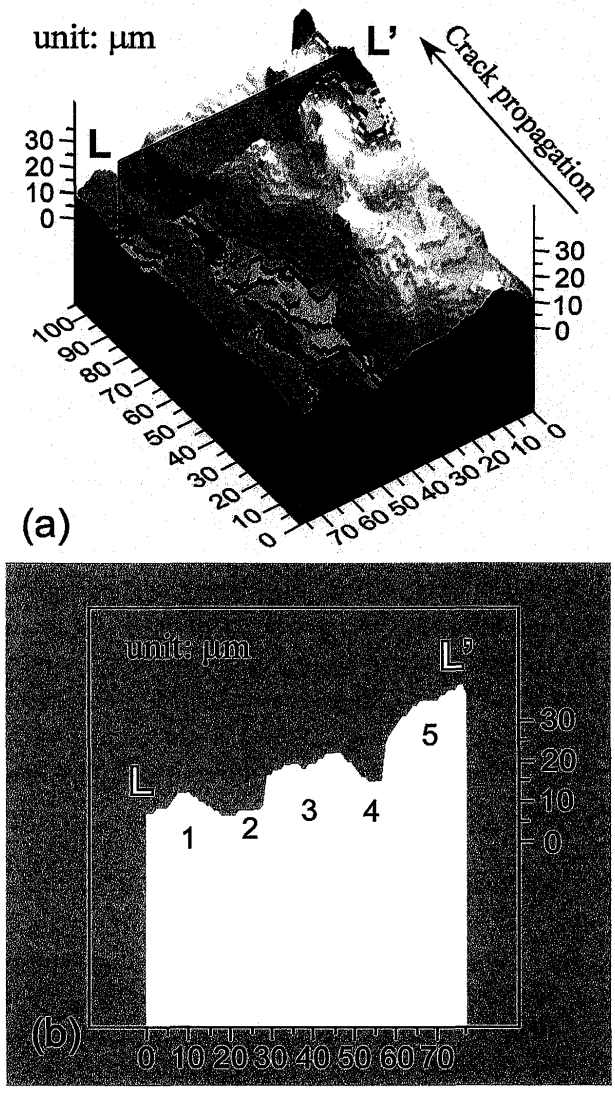

Fig.8 3-dimensional image of the fracture surface (a) and 2-dimensional image along cross section L-L' (b) for SUS329J1 base metal reheated at 1023K for 72ks.

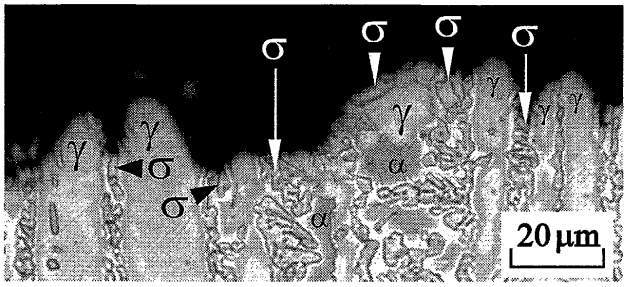

Fig.9 Cross sectional micrograph of fracture surface.

The nearly cross-sectional image was observed in order to reveal the effect of sigma phase on hydrogen induced cracking as shown in **Fig.9**.

According to microstructure observation, since many sigma phase sites were observed as well as many secondary cracks in the fracture surface as compared to as-received base metal, the reduction of tensile strength was mainly attributed to many secondary cracks associated with sigma phase.

In Fig.9, the sigma phase surrounded by elongated austenite became hollow. The sigma phase which was not surrounded by austenite was also observed at upper surface areas. It was assumed that this distribution morphology was attributted to this sigma phase itself, exfoliation and sigma/ferrite(α), or sigma/austenite phase boundaries exfoliation. The sigma phase was also observed at the bottom regions of the valley in another cross-sectional microstructure.

Hydrogen embrittlement was mainly attributed to either the cracking of sigma phase itself or the cracking of phase boundaries between sigma phase and another phase. As the result of these results, it was found that sigma phase and sigma/ferrite(α) phase boundaries were preferential hydrogen induced cracking sites, while austenite exhibited a small amount of plastic deformation because of lower susceptibility to hydrogen embrittlement.

4. Conclusions

(1) A small reduction of strength was recognized since a low level of hydrogen is sufficient to produce loss of strength in ferrite phase. The sigma phase enhanced hydrogen embrittlement.

(2) Since quasicleavage fracture in ferrite was dominant in the hydrogen embrittlement fracture surface, several flat steps with different elevations can be observed in 3-dimensional fracture surfaces of SUS329J1 base metal. It is also found that several flat hydrogen induced cracks propagated simultaneously into the interior of the specimen.

(3) The 3-dimensional image of the fracture surface containing sigma phase showed steep peaks and troughs although it looked like flat fracture surface. As a result of a study of the influence of sigma phase, it was found that sigma phase itself and sigma/ferrite(α) phase boundaries were preferential hydrogen induced cracking sites.

References

1) J.-O.Nilsson,"Overview Super duplex stainless steels", Materials Science and Technology, Vol.8, (1992), 685-699.

2) D.J.Kotecki, Ferrite control in duplex stainless steel weld metal, Weld. J. 10, (1986), 273s.

3) T.Kuroda, K.Bunno, T.Enjo, Effect of Microstructure on Hydrogen Embrittlement in Weld Heat-Affected Zone of Duplex Stainless Steel, J. Soc. Mat. Sci., Japan, 40-453, (1991), 730-735.

4) T.Kuroda, C.D.Lundin, Hydrogen Cracking of Duplex Stainless Steel Weldment, J. Soc. Mat. Sci., Japan, 43-488, (1994), 562-566.

5) T.Kuroda, K.Ikeuchi, K.Inoue, K.Nakade and Y.Kitagawa : Three-Dimensional Reconstruction System and Its Application to Fracture Surface of Stainless Steel, Quar. J. JWS, 20-1 (2001), 143-151. (in Japanese)

6) T.Kuroda, K.Ikeuchi, K. Nakade, K.Inoue, Y.Kitagawa : Three-dimensional Reconstruction of cleavage fracture surface for duplex stainless steel, VACCUM 65 (2002) 541-546.

7) T.Kuroda, K.Ikeuchi, K.Inoue, K. Nakade and Y. Kitagawa: Three-dimensional Reconstruction of Fracture Surface Using Area Matching Algorithm, Trans. JWRI, 30, (2001), No1.